The effect of propagation saw test geometries on critical cut length

Bastian Bergfeld[1]*, Karl W. Birkeland[2], Valentin Adam[1,3], Philipp L. Rosendahl[3], and Alec van Herwijnen[1]

[1] WSL Institute for Snow and Avalanche Research SLF, Davos, Switzerland
[2] Birkeland Snow and Avalanche Scientific, Bozeman, Montana
[3] Institute of Structural Mechanics and Design, Technical University of Darmstadt, Darmstadt, Germany

Correspondence to: Bastian Bergfeld (bastian.bergfeld@slf.ch)

Abstract:

For a slab avalanche to release, a crack in a weak snow layer beneath a cohesive snow slab has to initiate and propagate. Information on crack propagation is essential for assessing avalanche triggering potential. In the field, this information can be gathered with the Propagation Saw Test (PST), a field test that provides valuable data on crack propagation propensity. The first PSTs were performed about 20 years ago and standards have since been established. However, there are still differences in how the PST is performed. Standards in North America require the column ends to be cut vertically, whereas in Europe they are typically cut normal to the slope. In this study, we investigate the effect of these different column geometries on the critical cut length. To this end, we conducted 27 pairs of PST experiments, each pair consisting of one PST with slope normal cut ends and one PST with vertical cut ends. Our experiments showed that PSTs with normal cut ends have up to 50% shorter critical cut lengths, and the difference predominantly depends on the slope angle and slab thickness. We developed two load-based models to convert critical cut lengths between the test geometries: (i) a uniform slab model that treats the slab as one uniform layer and (ii) a layered model that accounts for stratification. For validation, we compare these models with a modern fracture mechanical model. For the rather uniform slabs of our experiments, both load-based models were in excellent agreement with measured data. For slabs with an artificial layering, the uniform load-model predictions reveal deviations from the fracture mechanical model whereas the layered model was still in excellent agreement. This study reveals the influence that the geometry of field tests and the slope angle of the field site have on test results. It also shows that only accurately prepared field tests can be reliable and therefore meaningful. However, we provide models to correct for imprecise field test geometry effects on the critical cut length.

KEYWORDS: stability test, Propagation Saw Test, edge effect, failure initiation

1 Introduction

Accurate assessment of fracture initiation and crack propagation is essential to evaluate the potential for triggering avalanches (Schweizer et al., 2016). In this context, the Propagation Saw Test (PST) is a field test that provides valuable insight into the propensity of cracks to propagate (Gauthier and Jamieson, 2006b). In the past 20 years several studies investigated the influence of PST geometry. They aimed to provide recommendations for the PST column length (Bair et al., 2014) or looked into the effect of changing slab thicknesses (Simenhois and Birkeland, 2008). It was also reported that the critical cut length depends on whether the ends of the PSTs are cut slope-normally or vertically (Gaume et al., 2017). Although PSTs have been used for approximately 20 years and utilized in various studies (Bair et al., 2013; Bergfeld et al., 2022; Bergfeld et al., 2021; Birkeland et al., 2019; Gauthier and Jamieson, 2008b), the lack of widely

accepted standards hinders its consistent and reproducible application across locations and practitioners. Standards in North America require the PST column ends to be cut vertically (CAA, 2016; Greene et al., 2022), whereas in Europe they are typically cut at a normal to the slope (Sigrist and Schweizer, 2007; van Herwijnen et al., 2016).

This methodological difference could possibly explain why previous studies were not conclusive as to whether the critical cut length decreases (Gaume et al., 2017, slope normal cuts) or increases (Gauthier and Jamieson, 2008a; McClung, 2009, both slope vertical cuts) with increasing slope angle. In both, North America and Europe the weak layer is most commonly cut upslope, but in rare cases, the weak layer is also cut downslope from the top. Gauthier and Jamieson (2006a) investigated this difference experimentally and observed no significant dependence of critical cut length on cutting direction. However, they also found that critical cut length does not depend on slope angle. Another contradictory statement about the cut length to slope angle relationship. However, the geometric and/or methodological differences (column geometry and cutting direction of PSTs) are likely to affect the results of PSTs (Gaume et al., 2017; Heierli et al., 2008, Supplement Figure S3). Our study aims to investigate the effect of different column geometries and cutting directions on the critical cut length, a major structural property. To achieve this, we conducted a series of side-by-side PST experiments with normal and vertical ends. In addition, we also investigated the influence of cutting direction (upslope or downslope).

The purpose of these experiments was to demonstrate the influence of PST column geometry and cutting direction on the critical cut length. We also explain where these differences come from and how the stratification of the snowpack influence these geometric effects. To this end, we developed a uniform- and layered load-based models to convert between PST geometries. In addition, the developed conversion models were validated against a modern fracture mechanics model (Rosendahl and Weissgraeber, 2020; Weißgraeber and Rosendahl, 2023).

2 Methods

Field Experiments

In January and March 2021, we performed field experiments above Davos in the Eastern Swiss Alps, and in Montana, United States. All field sites were around 2400 m.a.s.l. and PSTs resulted in all possible propagation outcomes (slab fracture, crack arrest and full propagation). In Davos, we tested a weak layer consisting of surface hoar (grain size: 2-4 mm), while in Montana the weak layer consisted of depth hoar (grain size: 1-4 mm) (Fierz et al., 2008). Slab thickness ranged from 52 to 96 cm.

In total 27 pairs of PSTs were performed, with each pair consisting of one test using slope normal ends (results with superscript X^N, Figure 1a) and the other with vertical ends (superscript X^V, Figure 1b). For three pairs, hence for six PSTs, we performed additional PSTs in which the weak layer was cut in downslope direction immediately next to the PST cut in the upslope direction (r_c^{up} and r_c^{down} in Figure 1b).
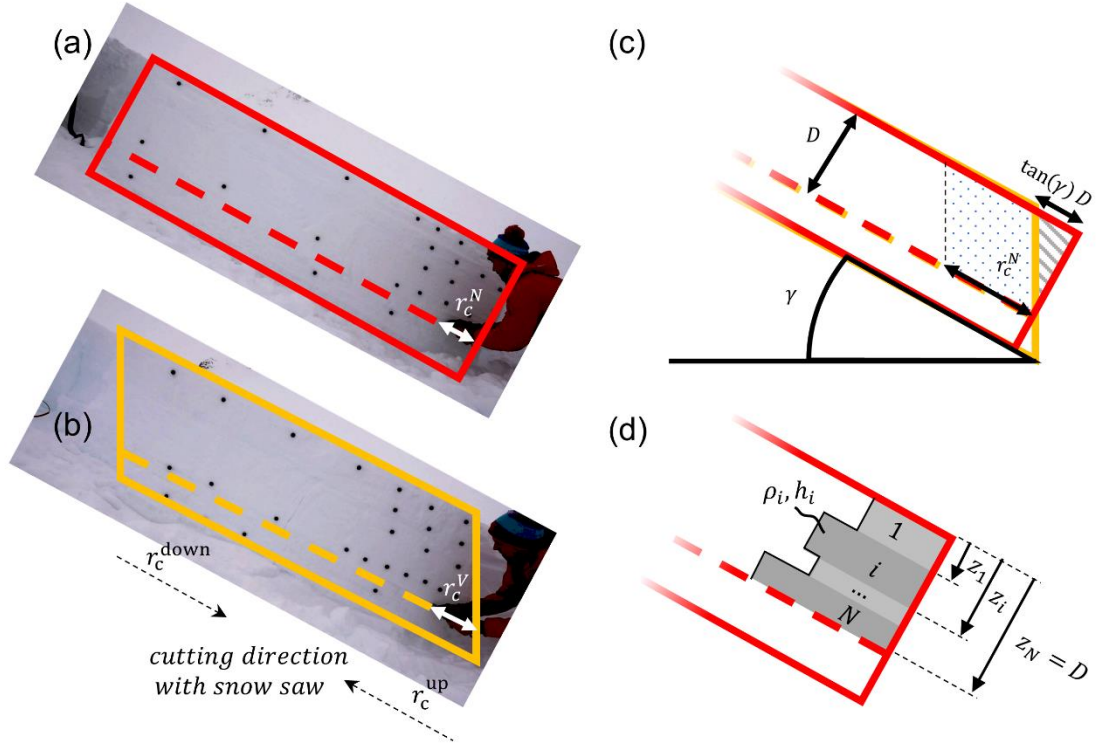
Figure 1: (a) PST with normal ends and a critical cut length r_c^N. The red outline indicates the PST geometry. The dashed line indicates the height of the weak layer. (b) PST with vertical ends and a critical cut length r_c^V. Additionally, the different cutting directions r_c^{up} and r_c^{down} are indicated. The two cutting directions were used in both PST geometries. (c) Difference in PST geometry at the downslope end of a PST. The main difference is the additional slab load for the slope normal geometry shown by the grey triangle. D is the slopenormal measured slab thickness and γ the slope angle. (d) In the layered load conversion model, each slab layer i (in both the vertical and normal PST configurations) contributes according to their density ρ_i, layer thickness h_i and depth in the slab z_i.

For all PSTs, we recorded the critical cut length as r_c^N for PSTs with normal ends, and r_c^V for vertical ends. We then compute the ratio of both cut lengths r_c^V/r_c^N. To investigate the effect of cutting directions, we used the ratio r_c^{up}/r_c^{down}, where r_c^{up} and r_c^{down} indicate whether the critical cut length was taken from upslope or downslope cutting of the weak layer, respectively (Figure 1b). Note that the ratio of the cutting direction was determined separately for the different PST geometries.

Conversion Models

Mechanically, cutting a PST can be modelled as a cantilever beam that does not deform sufficiently to come into contact with the snow under the cut. The cantilever (unsupported part of the slab) is loaded by the gravitational body forces, hence its own mass. This loading has to be carried through a combination of reaction forces (normal forces, shear forces, and bending moments inside the slab), which all work together to resist the load and maintain the slab's structural integrity. The stress transmitted from the slab to the foundation is known as bearing stress or contact stress. As the foundation is provided by the intact weak layer, the contact stress is transmitted right ahead of the saw cut. Generally, the contact stress has stress intensity close to the saw cut, it fades out away from the saw cut, and has normal and shear stress components.

However, the actual distribution of contact stress is similar in the slope-vertical and slope-normal PST geometry. Simplified, the contact stress is related to a reaction force of the weak layer which supports the cantilever. For a cantilever beam, the mixed-mode (normal and shear) reaction force R at the bedding is related to the total load of the unsupported part of the slab: $R = m\,g$, where m is the total mass of the slab above the saw cut and g is the gravitational acceleration. The maximum load a weak layer can support before fracture is reached at the critical cut length. Hence, also R is at a maximum at the critical cut length (R_{max}). In our load models, we assume that R_{max} is specific to a weak layer, which enables us to state that: $R_{max} = R_{max}^{V} = R_{max}^{N}$, where R_{max}^{V} and R_{max}^{N} are the reaction forces at the critical cut length which bear the unsupported portion of the slab in the slope-vertical and slope-normal PST geometry, respectively. As the gravitational acceleration is constant, the masses of the unsupported slab of the two PST geometries are equal:

$$m^{V} = m^{N} \qquad (1)$$

Note that the mass of the slab above the intact weak layer contributes to R_{max}, but since these are additive terms which are independent of PST geometry, they cancel each other out in equation 1.

Uniform Load Model (ULM). If we consider a uniform slab and express the mass m through snowpack properties equation 1 becomes:

$$\rho\,b\,r_c^{V}\,D = \rho\,b\,r_c^{N}\,D + \frac{1}{2}\tan(\gamma)DD\,\rho\,b \qquad (2)$$

where D is the slope normal measured slab thickness, γ the slope angle, b the PST column thickness and ρ the slab density (Figure 1c). After rearranging, equation 2 results in the following model for the conversion of critical cut lengths (assumption of a uniform slab):

$$r_c^{V} = r_c^{N} + \frac{\tan(\gamma)\,D}{2} \qquad (3)$$

At this point we would like to point out that this relationship (Equation 3) was already suggested in the context of anticrack nucleation. However, the derivation was based purely on geometric considerations and no further verification was carried out (Heierli et al., 2008, Supplement Figure S3).

Layered Load Model (LLM). The temporal sequence of weather conditions inevitably produces layered slabs in a natural snowpack. The individual layers differ, among other parameters, in their layer thickness and density. A sloped PST with layered slab in slope normal geometry results in more (compared to the ULM) load above the saw cut if high density layers are close to the snow surface (grey triangle in (Figure 1c and d). In addition to the slope angle γ, the extra load depends on the individual layer thickness h_i, density ρ_i, and on the relative depth z_i within the slab (Figure 1d). Conceptually, the layered load model is based on the same assumptions as the uniform load model. However, it considers the layering which makes the formulation to compute the additional load of PSTs with slope normal geometry more intricate:

$$r_c^{V} = \frac{\sum_{i=1}^{N} r_c^{N} h_i \rho_i + \frac{\tan(\gamma)}{2} h_i^{2}\rho_i + \tan(\gamma)\,(z_N - z_i)\,h_i\rho_i}{\sum_{i=1}^{N} h_i \rho_i} \qquad (4)$$

Where N is the number of layers. Hence for N = 1, equation 4 simplifies to the ULM (equation 3). For a detailed derivation of the layered load model, see Appendix A.

Layered Mechanical Model (LMM).

For further verification of the load models, we use a closed-form analytical model for layered snowpacks (Weißgraeber and Rosendahl, 2023) that was recently validated with field data (Bergfeld et al., 2023), has been utilized. This model describes the slab as shear-deformable, layered beam, and allows cylindrical bending, while the weak layer is represented

129   as a layer of smeared springs with a Young's and shear modulus. We used the model to determine the critical energy

130   release rate G_c from the measured critical cut length, depending of the geometric configuration (G_c^N or G_c^V, respectively).

131   This critical energy release rate, also called specific fracture energy, is a material property of the weak layer describing

132   its resistance to crack growth, and it is hence a proxy for the fundamental physical process of crack growth in PSTs.

133   Subsequently, we used the critical energy release rate determined from an experiment with slope normal beam ends to

134   calculate back to the critical cut length of a vertically cut PST. This model is therefore also suitable to convert a critical

135   cut length measured in one PST configuration to another. Compared to the ULM (Equation 3) and the LLM (Equation 4),

136   the LMM requires many more snowpack properties. However, it represents the specific snowpack layering of a PST and

137   its influence on the critical cut length in much more detail, as it takes into account the full deformation behaviour of the

138   slab and weak layer system. Uniform slabs or symmetrically (with respect to the centre height of the slab) layered slabs

139   are simplifications, usually slabs have a density gradient so that deeper layers have a higher density and are therefore

140   stiffer. However, the load models take very little account of the effects of asymmetric slab layering. We therefore used

141   the LMM to verify the influence of an asymmetrically layered slab on our load-based models (ULM, LLM).

Results

143   In total we performed 66 PSTs at four different field sites. 54 PSTs aimed to investigate the effect of PST geometry

144   (Appendix, Table C1), therefore the dataset include 27 pairs of PSTs and each pair consists of one PST with slope normal

145   and one with vertical PST beam ends. The remaining 12 PSTs were performed to investigate the difference between

146   upslope- and downslope cutting of a PST (Appendix, Table C2).

Normal vs. vertical PST ends

148   For upslope cutting, critical cut lengths were measured between 14 and 70 cm. Overall, r_c^V was systematically larger than

149   r_c^N, on average almost 50 % (colored boxes in Figure 2a).
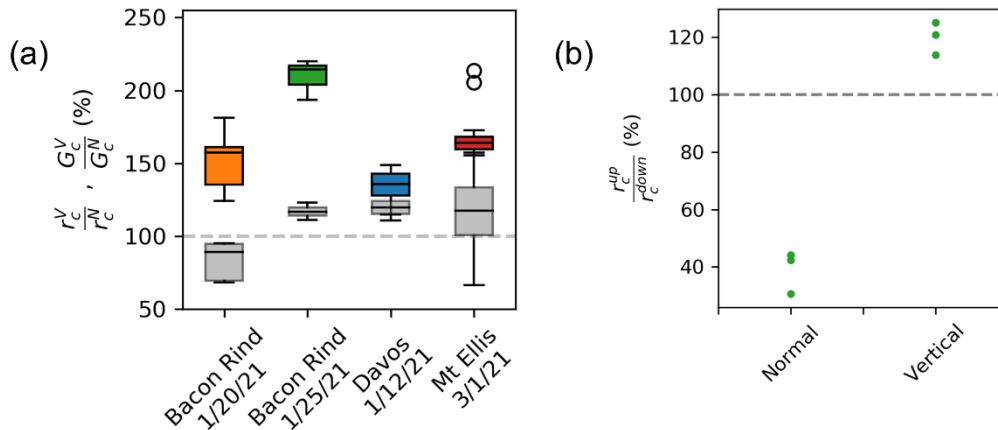
150

151   **Figure 2: (a) Ratio of critical cut lengths shown as boxplots for the different field days (colored). Ratio of the critical energy**
152   **release rates computed with the mechanical model using the critical cut lengths of the experiments (grey). Boxes represent the**
153   **inter-quartile range with the middle line representing the median value. (b) Ratio of critical cut length from PSTs with**
154   **downslope and upslope cuts. Results are shown for PSTs with normal and vertical PST ends. Both: The dashed line represents**
155   **a ratio of 1.**

156 Differences in snowpack conditions (e.g. slab thickness, layering, ...) at the various field sites resulted in different devi-
157 ations between PST geometries. Median ratios ranged from 136 % to 214 % (Figure 2a, horizontal lines in the colored
158 boxes).

Upslope vs. Downslope cutting

160 Beside PST geometry, the cutting direction also affects the critical cut length. For PSTs with normal ends, r_c^{up} was about
161 40% of r_c^{down} (Figure 2b, left), while for vertical PST ends r_c^{up} was about 20% longer than r_c^{down} (Figure 2b, right).
162 Again, these rather large differences can be explained by slab loading and slab mechanics as will be detailed in the dis-
163 cussions section.

Models

165 With Equations (3) and (4) we provide a **uniform load model** and a **layered load model**, respectively. The models allow
166 us to convert critical cut lengths between the different PST geometries. Our experiments show very good agreement with
167 both the uniform-load model (Figure 3a, dots) and the layered load model (Figure 3a, crosses). The RMSE between the
168 measured critical cut lengths in vertical geometry r_c^V and the modelled counterpart is 4.4 cm for the uniform load model
169 and 4.6 cm for the layered load model.
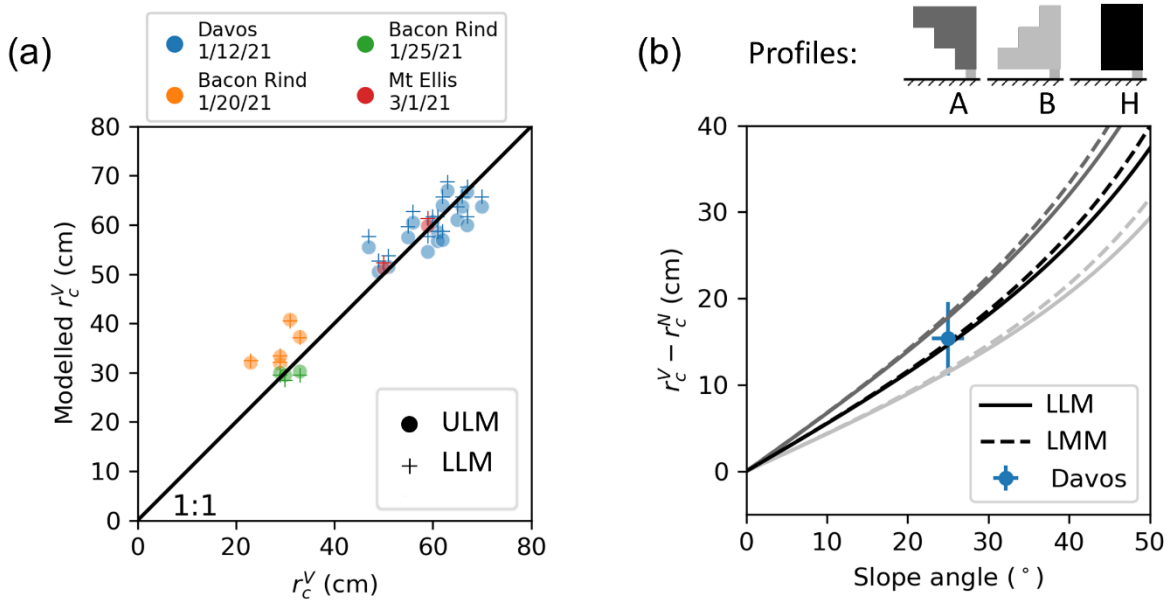
170
171 **Figure 3: (a) Modelled critical cut lengths for upslope cuts with vertical PST geometry r_c^V with the corresponding measured**
172 **values, dots represent the uniform load model (ULM, Equation 2) and pluses the layered load model (LLD, Equation 3). Dif-**
173 **ferent colors indicate the different field days. The black line is the 1:1 line and indicates a perfect model. (b) Modelled differ-**
174 **ences in critical cut lengths with slope angle (upslope cutting). The blue dot represents the mean and uncertainty of the meas-**
175 **urements in Davos, as this field day served to define the artificial profiles by matching the mean density. The solid lines are the**
176 **layered load model and the dashed lines result from the layered mechanical model (LMM). The grey shades indicate different**
177 **slab profiles given at the top of the figure.**

178 Using the **layered mechanical model** to analyse the global energy balance at the onset of crack growth, we derived
179 critical energy release rates from the experimental data. The model considers the layering and geometrical configuration
180 of a PST experiment to determine the critical energy release rate at the critical cut length, i.e., the specific fracture energy.
181 Unlike the critical cut length, the critical energy release rate is a material property of the weak layer and should thus not
182 depend on test geometry. In fact, the determined critical energy release rates, measured in the different PST configurations

183 (vertical or normal beam ends), differed by a maximum of 20% (Figure 2a, grey boxes), whereas the the critical cut length

184 were up to six times larger (Figure 2a, coloured boxes).

185

186 Our **uniform load model** considers a homogeneous slab and gives a tangential slope dependence (see Equation 3 and

187 black solid line in Figure 3b). For comparison, the **layered load model** and the **layered mechanical model** were evaluated

188 for many different slope angles (Figure 3b, solid and dashed lines, respectively) and 3 different generic slab configurations

189 (Figure 3b, top). In profile H the mean slab density matched the observed snow cover at our experiments in Davos. The

190 direct comparison for the artificial profile H shows a very good agreement between the load models and the mechanical

191 model (compare black solid line and black dashed line in Figure 3b). Note that for profile H the two load models are

192 equal. The deviations of the critical cut lengths ($r_c^V - r_c^N$) measured in Davos can be reproduced very accurately with all

193 models (Figure 3b, black lines and blue dot). In the asymmetric profiles A and B, additional artificial layers with the

194 minimum and maximum density of the Davos snow profile were inserted. For these highly asymmetric slabs (grey lines

195 in Figure 3) there are deviations between the models. Of course, the uniform model cannot represent any differences

196 induced by the layering. However, the layered load model and the mechanical model show good agreement over the entire

197 angle range, whereby the deviations slightly increase with increasing slope angles.

Discussion

Normal vs. vertical PST ends

200 PSTs with slope-normal and vertical ends showed large differences in the measured critical cut length. These differences

201 can be explained with the different PST geometries and the corresponding slab-induced loading of the weak layer. We

202 assume that PST beams were long enough, so that the tail end of the PST beam remains mechanically unchanged when

203 the saw cut is increased and is therefore not relevant (Bair et al., 2014). The constellation is as shown schematically in

204 Figure 1c. Even with no saw cut, the slope normal PST geometry already has an "unsupported" portion of the slab above

205 the weak layer (Figure 4a, blue area at the right beam end). This additional load, in normal geometry, generates higher

206 stresses in the weak layer (and higher energy release rate), leading to shorter critical cut lengths. The shorter critical cut

207 lengths can therefore easily be attributed to this additional load. However, the extent of the difference depends on snow-

208 pack properties (e.g. slab thickness, density layering) and slope angle.

209

210 This emphasizes that a measured critical cut length can only be interpreted for stability assessment if the applied geometric

211 PST configuration (including slope angle) is considered. In other words, our data show that two equal snowpacks, which

212 should exhibit a similar crack propagation propensity, likely result in completely different critical cut lengths depending

213 on how the PST beam ends were cut and on which slope angle the PST was performed. To ensure comparability of

214 measured critical cut lengths, it is thus imperative to account for the geometrical configuration and snowpack layering,

215 using the models presented.

Upslope vs. Downslope cutting

217 When cutting upslope, there is an additional part of the slab that induces an extra load on the weak layer in the slope

218 normal configuration (Figure 4a, blue area at the right beam end). When cutting from the top, however, a part of the slab

219   is missing, and there is less load (Figure 4a, blue area at the left beam end). The critical cut length of the upslope cut is

220   thus much shorter, in our experiments about 60% shorter (left side in Figure 2b).

221

222   In the vertical configuration, on the other hand, the load over the saw cut is always the same, independent of the cutting

223   direction. The observed differences, however, come from the differences in shear stress at the crack tip. Indeed, at the

224   weak layer, there are two shear stress components: (i) shear stress from the slope parallel gravitational pull on the slab

225   (Figure 4b, arrows in the middle), and (ii) bending induced shear stresses (Figure 4b, arrows at the left and right beam

226   end). The slope parallel gravitational pull is always in the same direction (downslope). The bending induced shear stresses

227   at the height of the weak layer, on the other hand, are always in the cut direction. When cutting the weak layer from the

228   bottom upwards, both contributions thus have an opposite effect and partially cancel each other out, while when cutting

229   from the top, both shear stresses have the same sign and add up. This results in longer critical cut lengths when sawing

230   upslope in vertical PSTs. In our measurements, these were 20% longer (right side in Figure 2b).

231
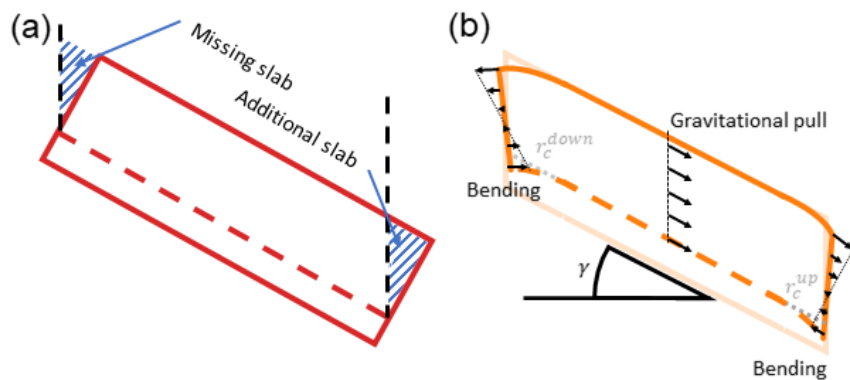
232

233   **Figure 4: (a) Schematic representation of a PST with normal ends and without a saw cut. The blue marked areas, at the right**
234   **and left of the PST beam, indicate the additional and missing slab load, respectively, relative to vertical ends (black dashed**
235   **lines). (b) PST with vertical ends and critical cut lengths r_c^{up} and r_c^{down} for upslope and downslope cutting, respectively. At**
236   **both PST beam ends the saw cut leads to bending, which results in a stress profile across the slab thickness (black arrows). In**
237   **the middle part of the PST, the black arrows represent stress in the slab due to the slope parallel gravitational pull. γ is the**
238   **slope angle.**

239

240   **Models**

241   Overall, the load models effectively explained our field results. (Figure 3a). If the RMSE of the uniform load- and layered

242   load model is compared, the uniform load model performs slightly better than the layered load model. However, since

243   our snowpack profiles show relatively homogeneous slabs without pronounced asymmetry (see Appendix D), we would

244   not attach any significance to this minor difference, especially for inhomogeneous and asymmetrical slabs. We believe

245   the layered load model is more aaccurate. This becomes clear in Figure 3b. Profiles A and B have a density gradient

246   within the slab (asymmetry). Deviations between the uniform and the layered load model seem plausible as higher density

247   layers which are close to the snow surface contribute more to the additional load present in slope normal PSTs (blue

248   hashed in Figure 4a) than if they are deeper in the snowpack. The difference in critical cut lengths is expected to be larger

249   (profile A) or smaller (profile B) than predicted by the uniform load model.

250

251   Beside the overall good conversion performance of the models, a systematic offset for PSTs from 20 January 2021 seem

252   to be present (orange dots in Figure 3). We suspect that in these PSTs the beam length was too short, the ratio between

253   slab thickness and beam length was only about 0.5 and the cut length to beam length ratio was 0.25. It is therefore very

254   likely that the geometric difference at the tail end of the beam was also relevant (Bair et al., 2014). However, this is not

255   considered in the models. Overall, our results thus show that the PST geometry plays an important role in the measured

256   critical cut length, and this is mostly driven by differences in load from the slab.

257

258   **Model application and limitation:**

259   PST datasets with different PST configurations can be homogenised using our models. This will increase the compara-

260   bility and ultimately the scientific utility of these datasets. In addition, it is often the case that the PST ends are cut

261   imprecisely (not perfectly vertical or slope normal) on inclined terrain. The angle of the free edge can easily be determined

262   from photos of the test, and a correction can then be applied using one of the load models with minor modifications

263   (Appendix B). The scatter of the experimentally determined critical cut lengths should thus be reduced.

264   Beside applications, shortcomings of the suggested load models are evident. Although, our experimental results show

265   that the relationship is sufficiently accurate for the conversion of PST geometries, additional changes (e.g. a different

266   slope anlges lead to different contributions of normal and shear loading of the weak layer, which may alter the critical

267   loading a weak layer can withstand. Ultimately, also influencing measured critical cut lengths) beyond the PST geome-

268   try are directly affecting model performance, so the relationship may no longer be sufficient. Imagine additional terms

269   from factors A and contributions B in Equation 1:

270   $A(\gamma, D, \dots)\ m^{\mathrm{V}} + B(\gamma, D, \dots) \propto A(\tilde{\gamma}, \tilde{D}, \dots)\ m^{\mathrm{N}} + B(\tilde{\gamma}, \tilde{D}, \dots)$

271   Both can have functional relationships on properties such as slope angle $(\gamma, \tilde{\gamma})$ and slab thickness $(D, \tilde{D})$.

272   As long as such properties remain unchanged $(\gamma = \tilde{\gamma}, D = \tilde{D})$, the additional terms cancel each other out and our load

273   models are applicable.

274   However, if the critical cut length measured at a certain slope angle and snow cover has to be transferred to a different

275   situation, the applicability of our models still needs to be confirmed with more experimental work. If necessary, the

276   functional relationships A and B will probably have to be identified and added. A more generally valid conversion for

277   critical cut lengths would be of great practical benefit as it allows to extrapolate measured point information on crack

278   propagation propensity to other slope areas where experimental work is not possible.

279   **Conclusion and Outlook**

280   This work has shown that the result of a PST, i.e., the measured critical cut length, is strongly influenced by the test

281   geometry and cutting direction. PSTs with slope normal beam ends (upslope cutting) systematically produce shorter crit-

282   ical cut lengths (48% on average). It also makes a significant difference whether the saw cut in a PST is made in the

283   upslope or downslope direction (deviations up to 60%). Both deviations can be explained mechanically and are largely

284   controlled by the difference in slab induced loads. Based on the slab load, a load model was derived for uniform, as well

285   as for layered slabs. Both models agree well with the experimental results. The comparison with a more sophisticated

286   validated fracture mechanical model shows good agreement between all models as long as the slab is largely homogene-

287   ous. For layered slabs, the uniform load model shows greater deviations. The layered load model, on the other hand,

288   shows only minor deviations. This demonstrates that the fracture mechanical model (LMM) is also largely load-driven in

289 this specific application. Overall, our results show that the interpretation of measured critical cut length in a PST is not
290 straightforward, as it is influenced by weak layer properties (specific fracture energy), slab properties (e.g. layering), and
291 test geometry.

292

293 Based on our findings, we show that PSTs with slope normal ends and a saw cut in upslope direction (Figure 1a) lead to
294 the shortest critical cut lengths. Hence, this procedure gives us the most conservative information on crack propagation
295 propensity (without post-processing). In addition, shorter critical cut lengths ensure that the overall column length is less
296 likely to influence test result. However, the disadvantage of this approach is the greater effect of slope angle on critical
297 cut lengths than for vertically cut PSTs. In order to compare tests on different slopes, this effect must be compensated for,
298 which is not yet straight forward. For an unbiased interpretation of PST results, experiments therefore need to be post-
299 processed before results from different snow packs, slope inclinations, etc. are compared or combined.

300

301 In general, the use of consistent PST standards will ensure that PST results are easy to interpret, will ensure scientific
302 rigor and will improve the comparability of tests and their results. In addition, standardization and conversion models
303 facilitate the comparison of results between researchers, leading to a deeper understanding of snowpack behavior. Prac-
304 titioners also benefit from standardized methods and interpretation aids that are invaluable in assessing avalanche risk
305 based on stability tests.

306

307 **Appendix A:**
308 The load above the saw cut of a PST with slope vertical geometry (V-PST) is independent of the slope angle. However,
309 the load of a PST with slope normal edges (N-PST) is not. In sloped terrain, a N-PST has more load above the saw cut
310 than a V-PST. The difference depends on the slope angle, but the layering also has an influence. Layers close to the snow
311 surface contribute more to the extra load than layers close to the weak layer (of the saw cut). In order to express the
312 relationship between critical cut lengths (r_c^V, r_c^N) the loads of layered snowpacks (m^V, m^N) have to be formulated through
313 density ρ_i, thickness h_i and the vertical location z_i of the slab layers i (Figure A1).

314
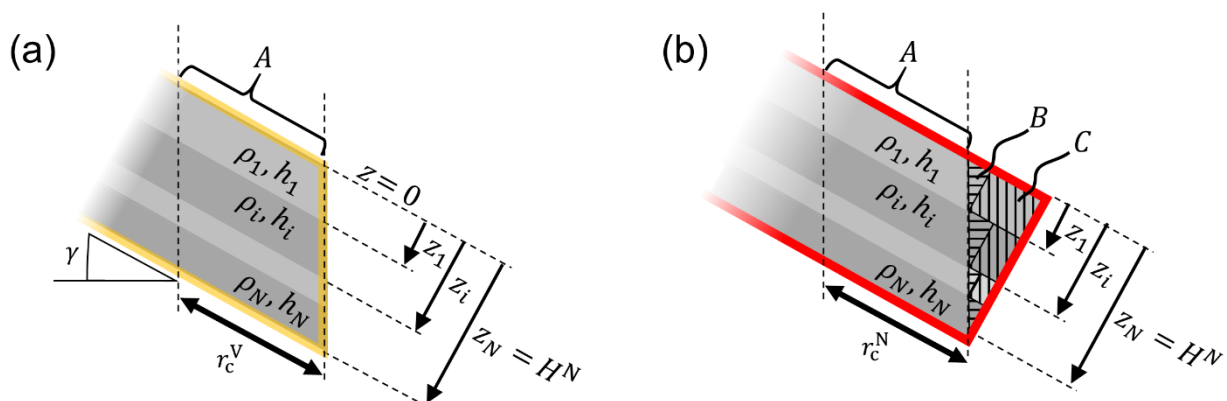
315

316 **Figure A1: (a) Schematic representation of a layered slab in a PST with slope vertical geometry (V-PST). (b) PST with slope**
317 **normal geometry (N-PST). In both cases, "A" indicates the volume of the slab above the saw cut r_c^Xa The mass of volume A**

318 **depends on column width b (not indicated), on r_c^X as well as the density ρ_i and thickness h_i of the slab layers i. In (b), the load**
319 **of the N-PST depends additionally on the slope angle as the Volumes B and C of each layer i increase with increasing angle.**

320 First for the simpler case of a V-PST (Figure A1a) the mass m^V is given by:

321
$$m^V = m_A = r_c^V\, b \sum_{i=1}^{N} h_i \rho_i \quad (A1)$$

322 In the N-PST the Volumes B and C also contribute to the overall mass located above the saw cut:

323
$$m^N = m_A + m_B + m_C \quad (A2)$$

324 The expression for the mass of Volume A remains the same as given in Equation A1. Now, however, the critical crack

325 length r_c^N is relevant instead of r_c^V. The masses m_B and m_C are given by:

326
$$m_B = \frac{1}{2}\,h_1{}^2 \tan(\gamma)\, b\rho_1 + \frac{1}{2}\,h_2{}^2 \tan(\gamma)\, b\rho_2 + \cdots + \frac{1}{2}\,h_N{}^2 \tan(\gamma)\, b\rho_N = \frac{b \tan(\gamma)\, \sum_{i=1}^{N} h_i{}^2 \rho_i}{2} \quad (A3)$$

327
$$m_C = (z_N - z_1) \tan(\gamma)\, h_1 b\rho_1 + (z_N - z_2) \tan(\gamma)\, h_2 b\rho_2 + \cdots + (z_N - z_N) \tan(\gamma)\, h_N b\rho_N$$

328
$$= b\tan(\gamma) \sum_{i=1}^{N} (z_N - z_i)\, h_i \rho_i \quad (A5)$$

329 Putting this together results in the overall mass of:

330
$$m^N = \tan(\gamma)\, b\, r_c^N \sum_{i=1}^{N} \frac{h_i \rho_i}{\tan(\gamma)} + \frac{h_i{}^2 \rho_i}{2\, r_c^N} + \frac{(z_N - z_i)\, h_i \rho_i}{r_c^N} \quad (A4)$$

331

332 Inserting in Equation A1 results in the layered load model providing the relation between the critical cut lengths r_c^V and

333 r_c^N:

334

335
$$r_c^V = r_c^N \frac{\tan(\gamma)\, \sum_{i=1}^{N} \dfrac{h_i \rho_i}{\tan(\gamma)} + \dfrac{h_i{}^2 \rho_i}{2\, r_c^N} + \dfrac{(z_N - z_i)\, h_i \rho_i}{r_c^N}}{\sum_{i=1}^{N} h_i \rho_i}$$

336
$$= \frac{\sum_{i=1}^{N} r_c^N h_i \rho_i + \dfrac{\tan(\gamma)}{2}\, h_i{}^2 \rho_i + \tan(\gamma)\, (z_N - z_i)\, h_i \rho_i}{\sum_{i=1}^{N} h_i \rho_i} \quad (A5)$$

337

338 **Appendix B:**

339 The equations derived in appendix A can be used to formulate a model to correct for imprecisely cut PST beam ends. E.g.

340 the sawing edge of a PST was close to cut slope normal, but with a deviation of angle β from slope normal (or vertical).

341 As a result, the critical cut length $r_c^{\tilde{N}}$ is measured in such an experiment. To account for this deviation, we have to add a

342 mass m_D in Equation A2. Note that this "mass" can be negative in the case β is negative (less overhanging mass than the

343 slope normal cut). The mass m_D has the same contributions as m_B and m_C but is computed from the angle of error β:

344
$$m_D = \frac{b \tan(\beta)\, \sum_{i=1}^{N} h_i{}^2 \rho_i}{2} + b\tan(\beta) \sum_{i=1}^{N} (z_N - z_i)\, h_i \rho_i \quad (B1)$$

345 At the end, the loads (Equation 1) provide the relation between the critical cut lengths:

346

347

348
$$m_A\!\left(r_c^{\tilde{N}}\right) + m_B + m_C + m_D = m_A(r_c^N) + m_B + m_C$$

349

$$\Rightarrow m_A(r_c^N) = m_A(r_c^{\tilde{N}}) + m_D \quad \text{(B2)}$$

351   By inserting the formulations for m_A (equation A1), the formula to correct an imprecisely cut N-PST is derived as:

$$r_c^N = \frac{r_c^{\tilde{N}} b \sum_{i=1}^{N} h_i \rho_i + b \tan(\beta) \sum_{i=1}^{N} \frac{h_i^2 \rho_i}{2} + (z_N - z_i) h_i \rho_i}{b \sum_{i=1}^{N} h_i \rho_i}$$

$$= r_c^{\tilde{N}} + \frac{\tan(\beta) \sum_{i=1}^{N} \frac{h_i^2 \rho_i}{2} + (z_N - z_i) h_i \rho_i}{\sum_{i=1}^{N} h_i \rho_i} \quad \text{(B3)}$$

354

Appendix C:

Table C1: Results of 27 pairs of PSTs, critical cut lengths r_c^V and r_c^N indicate whether PST beam ends were cut vertical or slope normal. Slab thickness H^N was measured in slope normal direction. Slope angle is provided in degrees. For further snowpack data we refer to the Appendix D.

PST-pairs	Location Date	Critical cut length r_c^V (cm)	Critical cut length r_c^N (cm)	Slab thickness H^N (cm)	Slope angle (°)
1	Davos 1.12.21	55 (±2)	43 (±2)	62 (±2)	25 (±2)
2	Davos 1.12.21	49 (±2)	36 (±2)	62 (±2)	25 (±2)
3	Davos 1.12.21	47 (±2)	41 (±2)	62 (±2)	25 (±2)
4	Davos 1.12.21	51 (±2)	37 (±2)	62 (±2)	25 (±2)
5	Davos 1.12.21	56 (±2)	46 (±2)	62 (±2)	25 (±2)
6	Davos 1.12.21	61 (±2)	45 (±2)	58 (±2)	25 (±2)
7	Davos 1.12.21	59 (±2)	41 (±2)	58 (±2)	25 (±2)
8	Davos 1.12.21	65 (±2)	47 (±2)	60 (±2)	25 (±2)
9	Davos 1.12.21	66 (±2)	49 (±2)	63 (±2)	25 (±2)
10	Davos 1.12.21	70 (±2)	49 (±2)	63 (±2)	25 (±2)
11	Davos 1.12.21	61 (±2)	42 (±2)	63 (±2)	25 (±2)
12	Davos 1.12.21	63 (±2)	52 (±2)	64 (±2)	25 (±2)
13	Davos 1.12.21	62 (±2)	42 (±2)	64 (±2)	25 (±2)
14	Davos 1.12.21	62 (±2)	49 (±2)	64 (±2)	25 (±2)
15	Davos 1.12.21	67 (±2)	45 (±2)	64 (±2)	25 (±2)
16	Davos 1.12.21	67 (±2)	51 (±2)	67 (±2)	25 (±2)
17	Davos 1.12.21	60 (±2)	45 (±2)	67 (±2)	25 (±2)
18	Bacon Rind 1.20.21	31 (±2)	25 (±2)	57 (±2)	29 (±2)
19	Bacon Rind 1.20.21	33 (±2)	21 (±2)	56 (±2)	30 (±2)
20	Bacon Rind 1.20.21	29 (±2)	16 (±2)	55 (±2)	30 (±2)
21	Bacon Rind 1.20.21	29 (±2)	18 (±2)	55 (±2)	29 (±2)
22	Bacon Rind 1.20.21	23 (±2)	17 (±2)	54 (±2)	29 (±2)
23	Bacon Rind 1.25.21	29 (±2)	15 (±2)	52 (±2)	30 (±2)
24	Bacon Rind 1.25.21	33 (±2)	15 (±2)	53 (±2)	30 (±2)
25	Bacon Rind 1.25.21	30 (±2)	14 (±2)	54 (±2)	30 (±2)
26	Mount Ellis 3.1.21	59 (±2)	38 (±2)	93 (±2)	25 (±2)
27	Mount Ellis 3.1.21	50 (±2)	29 (±2)	95 (±2)	25 (±2)

361 **Table C2: Critical cut lengths measured at Mount Ellis, Critical cut lengths r_c^{DOWN} and r_c^{UP} indicate if the weak layer was cut**
362 **downslope or upslope, respectively. Slab thickness H^N was measured in slope normal direction. Slope angle is provided in de-**
363 **grees. For further snowpack data we refer to the Appendix D.**

364

PST-pairs	Location Date	PST Geometry	Critical cut length r_c^{DOWN} (cm)	Critical cut length r_c^{UP} (cm)	Slab thickness H^N (cm)	Slope angle (°)
1	Bacon Rind 1.25.21	Slope normal	49 ($\pm$2)	15 ($\pm$2)	50 ($\pm$2)	30 ($\pm$2)
2	Bacon Rind 1.25.21	Vertical	24 ($\pm$2)	29 ($\pm$2)	52 ($\pm$2)	30 ($\pm$2)
3	Bacon Rind 1.25.21	Slope normal	29 ($\pm$2)	33($\pm$2)	54 ($\pm$2)	30 ($\pm$2)
4	Bacon Rind 1.25.21	Vertical	50 ($\pm$2)	50 ($\pm$2)	53 ($\pm$2)	30 ($\pm$2)
5	Bacon Rind 1.25.21	Slope normal	33 ($\pm$2)	14($\pm$2)	53 ($\pm$2)	30 ($\pm$2)
6	Bacon Rind 1.25.21	Vertical	24 ($\pm$2)	30 ($\pm$2)	53 ($\pm$2)	31 ($\pm$2)

365

366

 Appendix D:

 At each of our four field sites we took a manual profile including density measures. The following four figures are excerpts

 from the corresponding snow profile databanks.

 Figure D1: Manual profile taken at the Davos field site. The hashed area at the left site represents the hand hardness with snow
 height, the red line snow temperature with snow height. On the right side, grain type, grain size, hand harness, lemons and
 snow density are given. On the very right, stability test results are written at the height, of the tested weak layer.

375

Figure D2: Manual profile taken at the Bacon Rind field site on January 20ᵗʰ 2021. The blue area at the left site represents the hand hardness with snow height, On the right side, grain type, grain size, moisture and snow density are given. On the very right, stability test results are written at the height, of the tested weak layer.

Bacon Rind Sm Meadow **Karl Birkeland**
Madison Range-S **01/25/2021 - 12:00pm**
MT Co-ord: **44.84934N, -111.07942W**
Elevation: **2321 m** Slope Angle: **30°**
Aspect: **80°** Wind Loading:
Specifics: **We skied slope**

Stability: HS: **94** Layer Notes:
Air Temperature: 38-20cm: **Problematic layer**
Sky Cover: **CLR**
Precipitation: **NO**
Wind: **Calm**
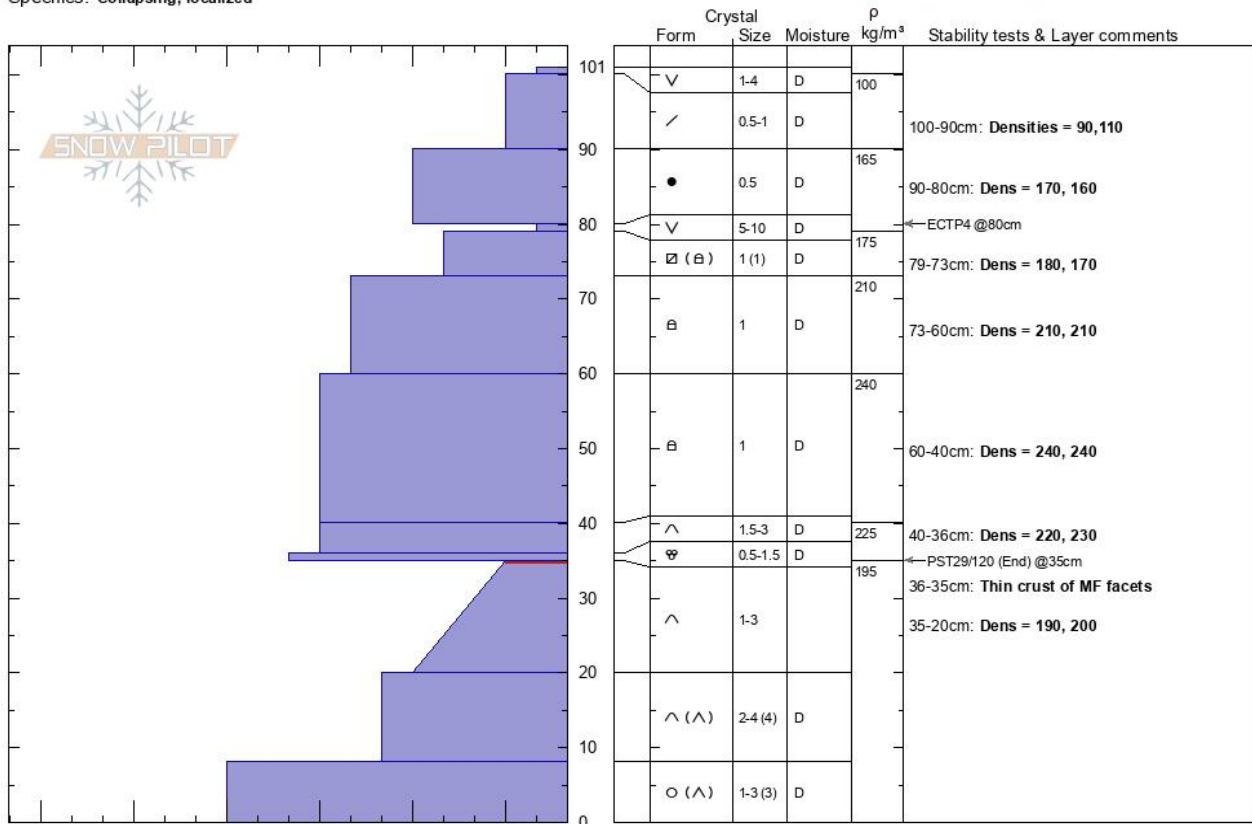
Notes: Pit dug to document snow conditions for research on PST geometry.
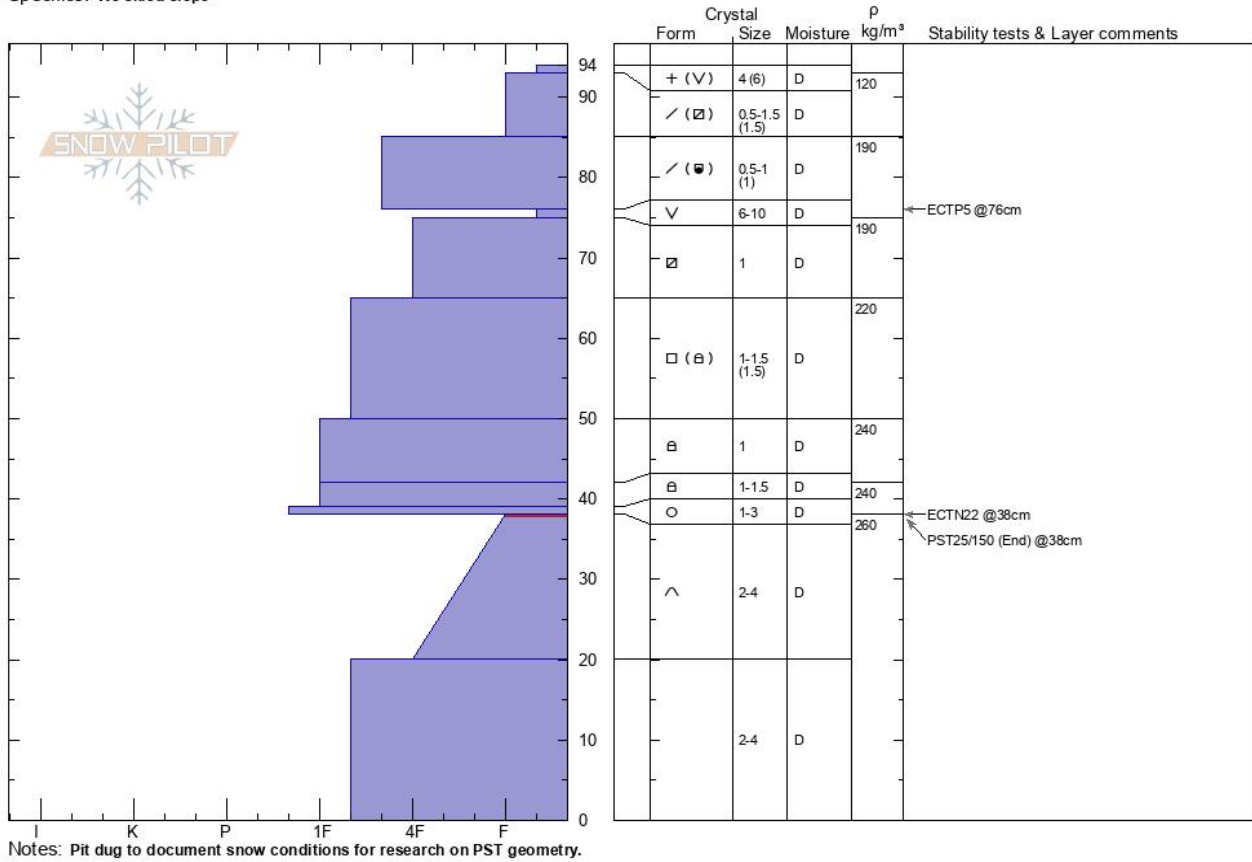
379

380 **Figure D3: Manual profile taken at the Bacon Rind field site on January 25th. The blue area at the left site represents the hand**
381 **hardness with snow height, On the right side, grain type, grain size, moisture and snow density are given. On the very right,**
382 **stability test results are written at the height, of the tested weak layer.**

383
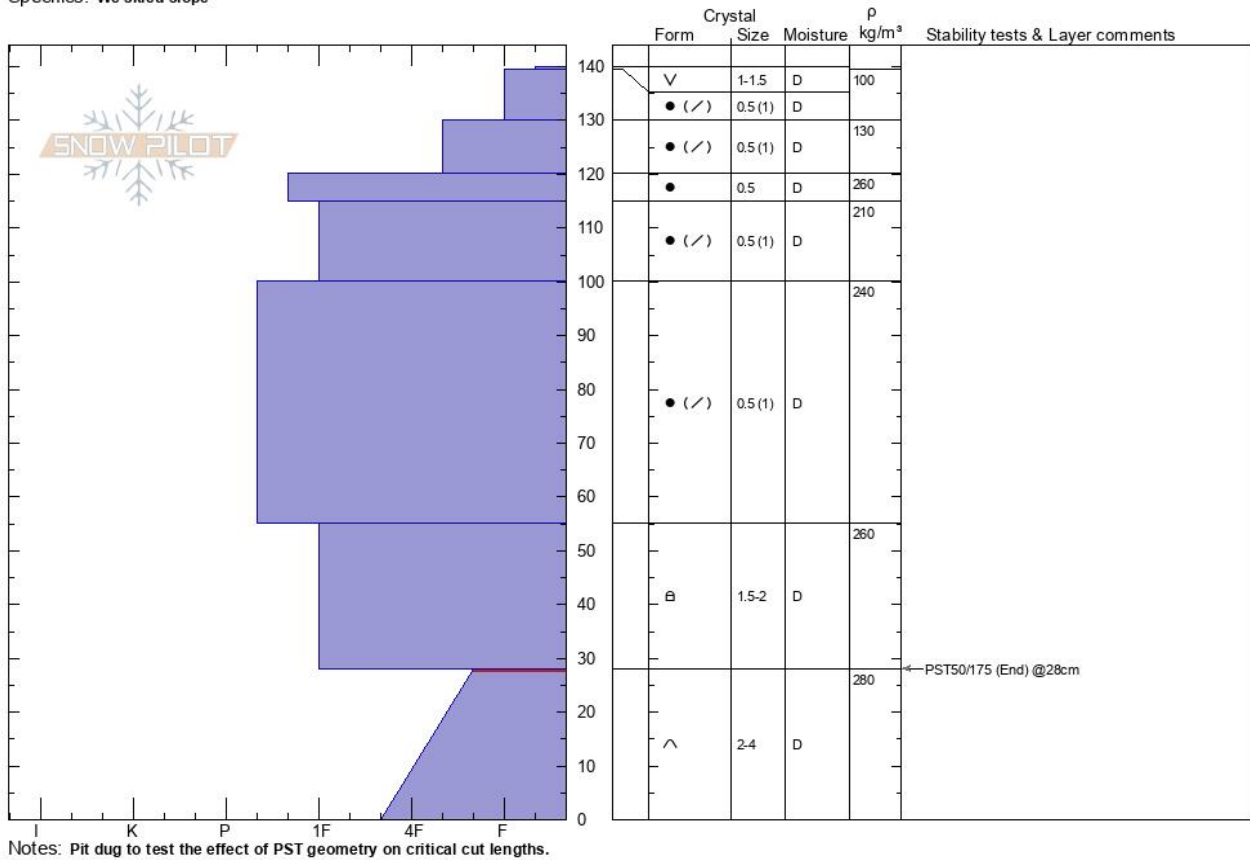
Figure D4: Manual profile taken at the Mount Ellis field site on January 25th. The blue area at the left site represents the hand hardness with snow height, On the right side, grain type, grain size, moisture and snow density are given. On the very right, stability test results are written at the height, of the tested weak layer.

Competing interests

The contact author has declared that none of the authors has any competing interests

Acknowledgement

We would like to thank Flavia Maeder, Erika Birkeland, and Alex Marienthal for assisting in the field. This research was partly supported by the Swiss National Science Foundation (grant no. 200021_169424) and funded by the Deutsche Forschungsgemeinschaft (DFG, German Research Foundation) under grant no. 460195514.

REFERENCES

Bair, E.H., Simenhois, R., van Herwijnen, A. and Birkeland, K., 2014. The influence of edge effects on crack propagation in snow stability tests. The Cryosphere, 8(4): 1407-1418.

Bair, E.H., Simenhois, R., van Herwijnen, A. and Birkeland, K.W., 2013. Edge effects in propagation tests. In: F. Naaim-Bouvet, Y. Durand and R. Lambert (Editors), Proceedings ISSW 2013. International Snow Science Workshop, Grenoble, France, 7-11 October 2013. ANENA, IRSTEA, Météo-France, Grenoble, France, pp. 335-356.

Bergfeld, B., van Herwijnen, A., Bobillier, G., Larose, E., Moreau, L., Trottet, B., Gaume, J., Cathomen, J., Dual, J. and Schweizer, J., 2022. Crack propagation speeds in weak snowpack layers. Journal of Glaciology, 68(269): 557-570.

Bergfeld, B., van Herwijnen, A., Bobillier, G., Rosendahl, P.L., Weißgraeber, P., Adam, V., Dual, J. and Schweizer, J., 2023. Temporal evolution of crack propagation characteristics in a weak snowpack layer: conditions of crack arrest and sustained propagation. Natural Hazards and Earth System Sciences, 23(1): 293-315.

Bergfeld, B., van Herwijnen, A., Reuter, B., Bobillier, G., Dual, J. and Schweizer, J., 2021. Dynamic crack propagation in weak snowpack layers: insights from high-resolution, high-speed photography. The Cryosphere, 15(7): 3539-3553.

Birkeland, K.W., van Herwijnen, A., Reuter, B. and Bergfeld, B., 2019. Temporal changes in the mechanical properties of snow related to crack propagation after loading. Cold Regions Science and Technology, 159: 142-152.

CAA, 2016. Technical Aspects of Snow Avalanche Risk Management—Resources and Guidelines for Avalanche Practitioners in Canada, Canadian Avalanche Association, Revelstoke, BC, Canada.

Fierz, C., Armstrong, R.L., Durand, Y., Etchevers, P., Greene, E., McClung, D., Nishimura, K., Satyawali, P.K. and Sokratov, S., 2008. The 2008 international classification of seasonal snow on the ground. In: C. Campbell, S. Conger and P. Haegeli (Editors), Proceedings ISSW 2008, International Snow Science Workshop, Whistler, Canada, 21-27 September 2008, pp. 579-580.

Gaume, J., van Herwijnen, A., Chambon, G., Wever, N. and Schweizer, J., 2017. Snow fracture in relation to slab avalanche release: critical state for the onset of crack propagation. The Cryosphere, 11(1): 217-228.

Gauthier, D. and Jamieson, B., 2008a. Evaluation of a prototype field test for fracture and failure propagation propensity in weak snowpack layers. Cold Regions Science and Technology, 51(2-3): 87-97.

Gauthier, D. and Jamieson, B., 2008b. Fracture propagation propensity in relation to snow slab avalanche release: Validating the Propagation Saw Test. Geophysical Research Letters, 35(13): L13501.

Gauthier, D. and Jamieson, J.B., 2006a. Evaluating a prototype field test for weak layer fracture and failure propagation. In: J.A. Gleason (Editor), Proceedings ISSW 2006. International Snow Science Workshop, Telluride CO, U.S.A., 1-6 October 2006, pp. 107-116.

Gauthier, D. and Jamieson, J.B., 2006b. Towards a field test for fracture propagation propensity in weak snowpack layers. Journal of Glaciology, 52(176): 164-168.

Greene, E., Birkeland, K.W., Elder, K., McCammon, I., Staples, M., Sharaf, D., Trautman, S. and Wagner, W., 2022. Snow, Weather, and Avalanches: Observation Guidelines for Avalanche Programs in the United States. American Avalanche Association, Denver CO, U.S.A., 110 pp.

Heierli, J., Gumbsch, P. and Zaiser, M., 2008. Anticrack nucleation as triggering mechanism for snow slab avalanches. Science, 321(5886): 240-243.

Jamieson, J.B. and Johnston, C.D., 1998. Refinements to the stability index for skier-triggered dry slab avalanches. Annals of Glaciology, 26: 296-302.

McClung, D.M., 2009. Dry snow slab quasi-brittle fracture initiation and verification from field tests. Journal of Geophysical Research-Earth Surface, 114: F01022.

Morin, S., Horton, S., Techel, F., Bavay, M., Coléou, C., Fierz, C., Gobiet, A., Hagenmuller, P., Lafaysse, M., Ližar, M., Mitterer, C., Monti, F., Müller, K., Olefs, M., Snook, J.S., van Herwijnen, A. and Vionnet, V., 2020. Application of physical snowpack models in support of operational avalanche hazard forecasting: A status report on current implementations and prospects for the future. Cold Regions Science and Technology, 170: 102910.

Richter, B., Schweizer, J., Rotach, M.W. and van Herwijnen, A., 2019. Validating modeled critical crack length for crack propagation in the snow cover model SNOWPACK. The Cryosphere, 13(12): 3353-3366.

Rosendahl, P.L. and Weissgraeber, P., 2020. Modeling snow slab avalanches caused by weak-layer failure - Part 1: Slabs on compliant and collapsible weak layers. The Cryosphere, 14(1): 115-130.

Schweizer, J., Reuter, B., van Herwijnen, A. and Gaume, J., 2016. Avalanche release 101. In: E. Greene (Editor), Proceedings ISSW 2016. International Snow Science Workshop, Breckenridge CO, U.S.A., 3-7 October 2016, pp. 1-11.

Sigrist, C. and Schweizer, J., 2007. Critical energy release rates of weak snowpack layers determined in field experiments. Geophysical Research Letters, 34(3): L03502.

Simenhois, R. and Birkeland, K.W., 2008. The effect of changing slab thickness on fracture propagation. In: C. Campbell, S. Conger and P. Haegeli (Editors), Proceedings ISSW 2008, International Snow Science Workshop, Whistler, Canada, 21-27 September 2008, pp. 755-760.

van Herwijnen, A., Gaume, J., Bair, E.H., Reuter, B., Birkeland, K.W. and Schweizer, J., 2016. Estimating the effective elastic modulus and specific fracture energy of snowpack layers from field experiments. Journal of Glaciology, 62(236): 997-1007.

Weißgraeber, P. and Rosendahl, P.L., 2023. A closed-form model for layered snow slabs. The Cryosphere, 17(4): 1475-1496.